Title

Interferometric spectroscopy with quantum light: Revealing out-of-time-ordering correlators

Journal

The Journal of Chemical Physics, 154(21)

ISSN

0021-9606

Authors

Asban, Shahaf
Dorfman, Konstantin E
Mukamel, Shaul

Publication Date

2021-06-07

DOI

10.1063/5.0047776

Interferometric-Spectroscopy With Quantum-Light; Revealing Out-of-Time-Ordering Correlators

Shahaf Asban,[1,*] Konstantin E. Dorfman,[2,†] and Shaul Mukamel[1,‡]

[1] *Department of Chemistry and Physics & Astronomy, University of California, Irvine, California 92697-2025, USA*
[2] *State Key Laboratory of Precision Spectroscopy, East China Normal University, Shanghai 200062, China*

We survey the inclusion of interferometric elements in nonlinear spectroscopy performed with quantum light. Controlled interference of electromagnetic fields coupled to matter can induce constructive or destructive contributions of microscopic coupling sequences (histories) of matter. Since quantum fields do not commute, quantum light signals are sensitive to the order of light-matter coupling sequence. Matter correlation functions are thus imprinted by different field factors, which depend on that order. We identify the associated quantum information obtained by controlling the weights of different contributing pathways, and offer several experimental schemes for recovering it. Nonlinear quantum response functions include out-of-time-ordering matter correlators (OTOC) which reveal how perturbations spread throughout a quantum system (information scrambling). Their effect becomes most notable when using ultrafast pulse sequences with respect to the path difference induced by the interferometer. OTOC appear in quantum-informatics studies in other fields, including black holes, high energy, and condensed matter physics.

I. INTRODUCTION

The quantum nature of light can affect and be utilized to steer optical signals in many ways [1]. First, unique properties such as photon entanglement show nonclassical bandwidth characteristics, offering new ways to study many-body correlations. Multi-photon collective resonances [2] excited by entangled light sources give access to matter information not available with classical sources. Second, low-intensity quantum light sources are useful for various sensing applications. An entangled pair can be generated such that each photon has a very different frequency regime. This provides a convenient way to probe matter information in less accessible frequency ranges (e.g. IR, XUV), while measuring visible photons [3]. Another property of quantum light is the larger parameter space which enables sensing applications such as phase imaging [4], quantum sensing networks , and spectrally resolved optical phase profiles [5]. Third, quantum light allows to extend nonlinear spectroscopic signals down to the few-photon level where the quantum nature of the field must be taken into account. Observed effects include the strong light-matter coupling in cavities [6], the enhancement of the medium's nonlinearity [7] and linear pump-signal scaling of the two-photon absorption processes [8]. The parameter-set of the photon wave-function offers novel control knobs that supplement classical parameters, such as frequencies and time delays [9]. Quantum light opens a possibility to shape and control excitation pathways of matter in a way not possible by shaped classical pulses, and results in steering exciton relaxation in molecular systems [**?**]. Fourth, quantum light sources enhance phase measurements beyond the shot-noise limit and have been recently shown experimentally to enhance the performance of imaging schemes [10]. The spatial resolution may be enhanced in quantum imaging applications, quantum-optical coherence, as well as in quantum lithographic applications. Quantum imaging with entangled light can achieve enhanced resolution, and quantum metrology can overcome the shot noise limit [11].

In this perspective, we survey emerging novel spectroscopic techniques made possible by interferometric setups. Each setup includes three components: an incoming quantum light source (preparation), field-matter coupling, and detection. Interference of optical fields has a rich history of experimentally unraveling illusive physical phenomena. Due to its linear dispersion, path differences of light are associated with time delays, rendering controlled interference setups (interferometers) valuable sensitive phase evaluation devices. Quantum probes are more complex and potentially carry additional information [12]. This can be used to outperform purely classical schemes in precision measurements, due to higher Fisher information and corresponding lower Cramér-Rao bound [13]. Setups based on Mach-Zehnder Rarity *et al.* [14], Hong-Ou-Mandel [15], and Franson [16] interferometers with quantum light are sensitive to the change in photon statistics of quantum light upon coupling to matter, and can be revealed by coincidence detection with multiple detectors [16–18]. Quantum-enhanced interferometers – such as the ones used for the observation of gravitational waves [19, 20] – indeed demonstrate unprecedented phase estimation precision with high loss tolerance at lower photon flux [21–25], and in wide-field imaging [26]. Generally, interferometers shuffle the time ordering of the input fields, creating a superposition of possible histories related to different paths. When the input field is a com-

* sasban@uci.edu
† dorfmank@lps.ecnu.edu.cn
‡ smukamel@uci.edu

position of well separated pulses, this effect is expressed in the output of time- resolved signals. This superimposed re-ordering can be described via linear transformations, and further classified into symmetry groups (Sec. II), suggesting a systematic classification of experimental setups. Here, we consider coupling a quantum material system of interest, to auxiliary electromagnetic fields under such conditions. The probe may propagate through known interference at any stage – prior, during or after the coupling with matter – and finally detected. Our approach [27] is closely related to the space-time tomographic mapping of superdensity operators [28]. We connect quantum information contributions to matter quantities.

Matter does not affect the state of coherent light, thus, all light-matter coupling histories (Liouville pathways) contribute with the same weight of the field. Their sum defines the classical response function. In contrast, other states of light (e.g., fixed number of photons) may carry different amplitude for each possible pathway. Each light-matter interaction sequence is then associated with a unique generalized response, which constitutes the classical (nonlinear) response [29–31]. From this point of view, the excess (quantum) information carried by the probe, allows one to open the measurement black box and closely observe the triggering sequence. Interferometric transformations of such states of light, correspond to altering between superimposed pathways judiciously (in lossless transformations). The interference of classical probes results in an output modulated by the classical response. The algebraic-geometric view of interferometry, implies that invariant observables transform as scalars (e.g., total photon number) and thus detected as constant flux. Others, (e.g., single polarization after basis transformation) are sensitive to rotations and thus show oscillations in measurements [32, 33]. The latter may carry useful information and should be studied in more detail.

The response to classical light is given by correlation functions of the dipole operator $V(t_n)\,V(t_{n-1})\ldots V(t_1)$ with a specific prescription of time ordering, we label them time ordered correlators (TOC). Multiphoton interferometric signals can give rise to generalized response functions, composed of light-matter coupling sequences in irregular time-ordering. These are broadly denoted out-of-time-ordering correlators (OTOC). This terminology will be precisely defined in Sec. III A. OTOC are attracting considerable attention in other fields, connected to quantum information dynamics of interacting many-body (closed) systems [34–51]. They provide useful signatures of quantum information scrambling, motivated by the quantum analogue of the "butterfly effect". In chaotic quantum systems, they grow exponentially fast (in time) prior to the Ehrenfest time (timescale in which quantum effects dominate) [34, 35, 39, 52, 53]. Otherwise, it follows a powerlaw at most [41, 43, 44]. Computation of multipoint space-time correlations in such setups can be carried out using the density operator formalism in Liouville space, introduced in [27] and more recently in [28]. Alternatively, it can be done using the wave-function (Hilbert space) approach [39]. The latter circumvents perplexing paradoxes one would inevitably encounter in *time symmetric* formulations to quantum mechanics [54, 55].

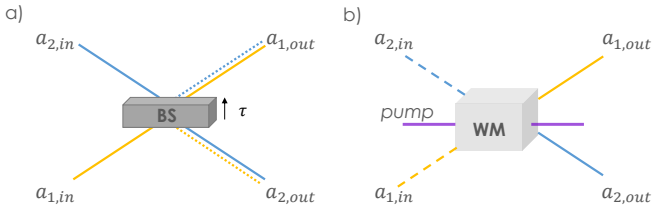

Figure 1. Interferometric elements. (a) Passive interferometric element, used to combine two incoming modes to superposed outgoing modes with the input output relation given by Eq. 1, where $\phi = \omega\tau$. (b) An active interferometric element, involves a nonlinear parametric process such as three-wave mixing, and four-wave mixing. Dashed lines represent modes that are initially in the vacuum state. In four-wave mixing, one of the inputs is populated, e.g., attenuated pump as in Eq. 4.

In Sec. II we describe the building blocks of linear and nonlinear interferometry. In Sec. III we present a general expression for the observable in Liouville space. In III A we discuss the contributions of OTOC obtained by post-coupling interferometry (detection). We then introduce novel pathway selection protocols such as exchange-phase cycling in Sec. III B, and time domain sorting in Sec. III C – both enabled by state-preparation in interferometric setups. We discuss an approach for harnessing Einstein-Podolsky-Rosen (EPR) correlations for enhanced joint time-frequency resolutions in Sec. III D. Finally we summarize our results in Sec. IV.

II. BUILDING BLOCKS OF NTERFEROMETRIC SIGNALS

Interferometry can be classified into two main types: passive-linear or active-nonlinear wave-mixing. Introducing a group-theoretic description of the interferometric elements, reveals clear notions regarding available information in terms of conserved currents. Matter degrees of freedom may introduce broken symmetries, altering otherwise-invariant quantities in terms of photon flux. We consider optical modes described by boson annihilation (creation) operators a_i $\left(a_i^\dagger\right)$, satisfying $\left[a_i, a_j^\dagger\right] = \delta_{ij}$ and $[a_i, a_j] = 0$. In order to discuss their transformations under interferometric setups, we adopt the vector notation $\boldsymbol{a} \equiv (a_1, a_2)^T$.

A. Linear-passive interferometric elements

A generic linear interferometric setup is realized by arrays of beam-splitters (BS) as depicted in Fig. 1a, mirrors and phase elements. The input-output relations corresponding to the two-port device (BS) is described by the unitary transformation $\boldsymbol{a}_{\rm out} = \hat{\mathcal{R}}_\phi \boldsymbol{a}_{\rm in}$ and

$$\hat{\mathcal{R}}_\phi = \begin{pmatrix} T & iRe^{i\phi} \\ iRe^{-i\phi} & T \end{pmatrix} \tag{1}$$

Here T and R are the reflection and transmission coefficients such that $T^2 + R^2 = 1$, and ϕ is a relative phase employed e.g., by shifted BS or mirrors (assuming lossless BS). Such elements are employed in many interferometric schemes – historically highlighting different physical realizations(i.e., Mach-Zehnder, Franson, Michelson Sagnac, relying on combinations of optical modes). The symmetry group of such transformations becomes more apparent by introducing the Hermitian operators [56]

$$J_x = \frac{1}{2}\left(a_1^\dagger a_2 + a_2^\dagger a_1\right), \tag{2a}$$
$$J_y = -\frac{i}{2}\left(a_1^\dagger a_2 - a_2^\dagger a_1\right), \tag{2b}$$
$$J_z = \frac{1}{2}\left(a_1^\dagger a_1 - a_2^\dagger a_2\right), \tag{2c}$$

satisfying the commutation relations of the Lie algebra of $SU(2)$, $[J_i, J_j] = i\epsilon_{ijk}J_k$, where ϵ_{ijk} is the antisymmetric tensor and and $i, j, k \in x, y, z$ (the number operator $N = a_1^\dagger a_1 + a_2^\dagger a_2$ is proportional to the identity). Clearly, two-mode passive rotation corresponds to an $SU(2)$ transformation with the invariant (Casimir) $J^2 = \frac{N}{2}\left(\frac{N}{2}+1\right)$. Coupling to matter degrees of freedom in the interaction picture, is represented by a relative shift in the unitary evolution. This stems from the fact that for each path, the joint light-matter system is evolved for different duration, giving rise to the out-of-time-ordering matter correlators (OTOC) and discussed in Sec. III A. The evolution operator is given by $\hat{U}(t, t') \equiv \exp\left\{-\frac{i}{\hbar}H(t - t')\right\}$, where $H = H_\phi + H_\mu + H_{\mu\phi}$. In the absence of matter, the path difference merely yields a linear phase $\phi = \omega\tau$ corresponding to time translations of the combined modes.

B. Nonlinear-active interferometric elements

Active interferometric elements constitute nonlinear combinations of fields, e.g., n-wave mixing processes. Three-wave mixing generates entangled photon pairs through parametric down conversion. A pump photon is down converted to a pair of spontaneously generated entangled photons. Four-wave mixing (FWM) induces further quadrature squeezing Reid and Walls [57], which attracted considerable attention from the early days of quantum enhanced metrology, aiming to improve the detection of gravitation wave Caves [19].

Nonlinear interferometric techniques present several merits. They utilize remarkable bandwidth extension with narrowband probes Shaked *et al.* [25], improved contrast in phase measurements with sub-shotnoise scaling – while maintaining these enhanced features with impressive loss tolerance Hudelist *et al.* [21], Li *et al.* [22], Anderson *et al.* [23], Manceau *et al.* [24], Frascella *et al.* [26], Du *et al.* [58]. It can be employed in the detection process to characterize time-domain light-matter pathways as further discussed in Sec. III C.

To characterize a two-photon FWM operation in terms of a transformation, we introduce the operators

$$K_x = \frac{1}{2}\left(a_1^\dagger a_2^\dagger + a_1 a_2\right), \tag{3a}$$
$$K_y = -\frac{i}{2}\left(a_1^\dagger a_2^\dagger - a_1 a_2\right), \tag{3b}$$
$$K_z = \frac{1}{2}\left(a_1^\dagger a_1 + a_2 a_2^\dagger\right), \tag{3c}$$

satisfying the of the Lorentz group $SU(1,1)$; $[K_x, K_y] = -iK_z$, $[K_y, K_z] = iK_x$ and $[K_z, K_x] = iK_y$, and the Casimir (invariant) $K^2 = J_z(J_z + 1)$. To demonstrate their effect, we consider a realization of this transformation in which one of the inputs in Fig. 1b is populated by an attenuated pump, with a relative delay δ with respect to the activating pump. The scattering matrix is then given by

$$\begin{pmatrix} a_1 \\ a_2^\dagger \end{pmatrix}_{\rm out} = \begin{pmatrix} \cosh\beta & e^{-i\delta}\sinh\beta \\ e^{i\delta}\sinh\beta & \cosh\beta \end{pmatrix} \begin{pmatrix} a_1 \\ a_2^\dagger \end{pmatrix}_{\rm in}, \tag{4}$$

where β is related to the reflectivity of the FWM Yurke *et al.* [56]. The J operators transform under the passive elements using $SU(2)$ rotations which are (almost) equivalent to manifold-preserving rotations in 3D. In contrast, the active elements impose Lorentz boosts on the K operators which corresponds to quadrature squeezing (manifold-shearing). In addition to the benefits derived from narrowband pump operation (above), high-order mixing generate particularly useful set for sorting through individual spontaneous processes (Sec. III C).

III. INTERFEROMETRIC QUANTUM SPECTROSCOPY – AN OPEN FRONTIER

Quantum fields are represented by operator quantities, in contrast to classical fields, which are c-numbers. Pertubative expansion of field-matter interactions yields optical signals expressed as multi-point correlation functions. The relative order of the dipole operators impacts the detected time ordering of the field-matter interactions and their expectation values. For non commuting fields, each arrangement of matter correlation function corresponds

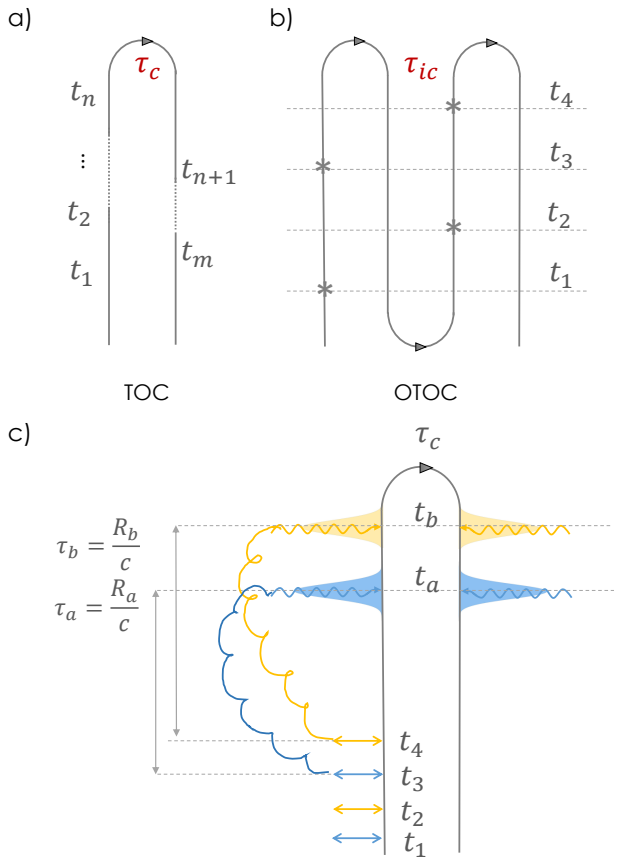

Figure 2. **Time-ordered Vs. out-of-time-ordering matter correlators**. (a) A fully time-ordered matter correlator (TOC) computed along a typical closed time contour τ_c. Such contribution compose the nonlinear response of matter upon coupling to classical light. (b) An OTOC diagram. Different optical paths in the interferometer re-arrange the radiative trajectories in the detection plane. The resulting OTOC are computed along an irregular wiggling time contour τ_{ic}. (c) A fully time-ordered loop diagrammatic representation of a possible process that contributes to the 4^{th} order optical signal. Two photons interact with a sample, then detected in coincidence following free propagation duration of τ_a and τ_b. The correlators are computed along the closed time contour τ_c from the distant past to the present back to the past.

to a different field correlation function. Thus, various detection schemes, can provide different information regarding the many-body dynamics.

Interferometric setups typically mix several modes and thus the mapping between physical interaction occurrences and their detection time is not straightforward. Below, we survey several approaches to manipulate and distinguish between time ordered events, and show how OTOC show up in measurements.

A. Out-of-time-ordering correlators – order of arrival Vs. order of interaction

When a quantum system is coupled to a classical field the, response is given by correlation functions of the form $\langle V(t_m)\cdots V(t_{n+1})\,V(t_n)\cdots V(t_2)\,V(t_1)\rangle$ represented by the loop diagram in Fig. 2a. Time proceeds forward in the left branch from t_1 to t_n, then proceeds backward on the right branch from t_{n+1} to t_m. We denote these time ordered correlators (TOC). Interferometric measurements with quantum light are given by more complex objects where time proceeds forward and backward multiple times, as shown in Fig. 2b. These are denoted OTOC.

As an example we consider the loop diagram shown in Fig. 2c. Matter correlation function in this example can be read off the diagram as $\langle \mathcal{T}_c V(t_4)\,V(t_3)\,V(t_2)\,V(t_1)\rangle$, where $\mathcal{T}_c$ is a time ordering operator corresponding to the closed time contour τ_c. Light-matter interaction events are ordered along the loop, and propagated forward in time from the distant past on the left branch, and backwards in time to the past on the right branch. In this example, $t_4 > t_3 > t_2 > t_1$ such that the propagation is always forward in time as depicted in Fig. 2c. An OTOC appears when the time-flow may be inverted backwards in some intervals of the correlation function, e.g., $\langle \mathcal{T} V(t_4)\,V(t_2)\,V(t_3)\,V(t_1)\rangle$, which yields reverse evolution between the second and third operators and depicted in Fig. 2b. Two-photon input in an interferometer introduces several modified time-orderings, resulting in irregular time-flow at the output. The coupling of light with matter parametrizes the matter correlation functions along the wiggling contour such as the one introduced in Ref. [39] for computations of OTOC in closed systems. This can be interpreted as interference of past and future contributions of matter multipoint correlation functions. However, this terminology can be avoided. We next review the interferometric transformation in terms of the detected signal.

When the electromagnetic field propagation direction is known, the Jordan-Schwinger map (JSM) is described by Stokes operators which follow the Lie algebra of $SU(2)$ symmetry group [56, 59–61]. Thus, (passive) interferometric setups can be described using a sequence of $SU(2)$ rotations (see Sec. II). The Hong-Ou-Mandel (HOM) interferometer depicted in Fig. 3 [62], is the simplest setup that gives rise to interference between future and past matter events. It combines two optical modes on a movable BS, which are then detected in coincidence using two detectors. The shift of the BS with respect to the center introduces controlled path differences between four distinct trajectories. Observables in this setup are composed purely of field operators that evolve according to the free electromagnetic Hamiltonian H_ϕ. Measurements are described using annihilation of modes in the far-field basis (post-rotation) as described by Glauber [63].

The light-matter coupling $H_{\mu\phi}$ is generally composed

of operators from the joint Hilbert space. Light and matter degrees of freedom thus become entangled upon energy exchange. We consider an optical signal, generated from a general multipoint correlation function of field operators, given by (see Sec. S2 of the SM)

$$\mathcal{C}(t_1,...,t_n)=\left\langle \mathcal{T}\mathcal{O}_{t_1,...,t_n}\left(\boldsymbol{\mathcal{E}},\boldsymbol{\mathcal{E}}^{\dagger}\right)e^{-\frac{i}{\hbar}\int_{t_0}^{t}du\mathcal{H}_{\mu\phi,-}(u)}\right\rangle. \quad (5)$$

Here $\mathcal{C}(t_1,...,t_n)$ is an n-point correlation function where t is taken to be the latest time, $\mathcal{T}$ is the time-ordering superoperator, $\mathcal{O}_{t_1,...,t_n}$ is a superoperator composition of the electric field operators in Liouville space and $\langle\cdots\rangle\equiv\mathrm{tr}\{\cdots\rho(t_0)\}$ is the trace with respect to the initial state of the density operator. $\mathcal{H}_{\mu\phi,-}(t)$ is the interaction superoperator operating on a Hilbert space operator A as a commutator $\mathcal{H}_{\mu\phi,-}A\equiv\mathcal{H}_{\mu\phi}A-A\mathcal{H}_{\mu\phi}$ Mukamel [27]. $\boldsymbol{\mathcal{E}}\left(\boldsymbol{\mathcal{E}}^{\dagger}\right)$ is the positive (negative) frequency electric field components $\boldsymbol{E}=\boldsymbol{\mathcal{E}}+\boldsymbol{\mathcal{E}}^{\dagger}$. In the following illustration we are interested in expectation values of intensity correlations. To that end it is convenient to introduce the right-left superoperator notation, whereby left (right) superoperators $\mathcal{E}_L(\mathcal{E}_R)$, act on the density according to $\mathcal{E}_L\rho\equiv\mathcal{E}\rho$ $(\mathcal{E}_R\rho\equiv\rho\mathcal{E})$. One can calculate the observables according to *order of arrival* at the detector, imposing the coupling description in this basis, $\boldsymbol{\mathcal{E}}_{\text{detection}}=\hat{\mathcal{R}}\boldsymbol{\mathcal{E}}_{\text{interaction}}$. Alternatively, the observable can be computed in the *order of interaction* with matter, in which $\mathcal{O}_{t_1,...,t_n}\left(\boldsymbol{\mathcal{E}},\boldsymbol{\mathcal{E}}^{\dagger}\right)$ will be expressed in basis of the interaction operators (rotation backwards, see Sec. S2 of the SM). In this description, the high dimensional space – accommodating both the electromagnetic field and the matter field of dim $H_\mu\oplus H_\phi$ – is unraveled by fully time-ordered correlation functions in the interaction picture. Since only part of the system (i.e. the electromagnetic field) is detected, path difference of the auxiliary degrees of freedom correspond to effective time-flow wiggling in the measured matter correlation function. When the observable $\mathcal{O}\left(\boldsymbol{\mathcal{E}},\boldsymbol{\mathcal{E}}^{\dagger}\right)$ is invariant under rotations (scalar e.g., $\boldsymbol{\mathcal{E}}^{\dagger}\cdot\boldsymbol{\mathcal{E}}$, or any function of the Casimir of the Stokes operators), no interference will be registered in the absence of matter. When the observable is basis dependent, interference between future and past matter pathways may show up in coincidence counting experiments. Notably, this is also where one would look for superior quantum performance with respect to phase-shift measurements [56].

Example of an OTOC contribution

Consider the setup sketched in Fig. 3. Two modes $\{E_a,E_b\}$ are prepared with a relative delay time τ, then interact with a sample. The modes are rotated by a BS and measured in coincidence respectively at space-time coordinates $\{\boldsymbol{r}_at_a,\boldsymbol{r}_bt_b\}$. The recorded signal can

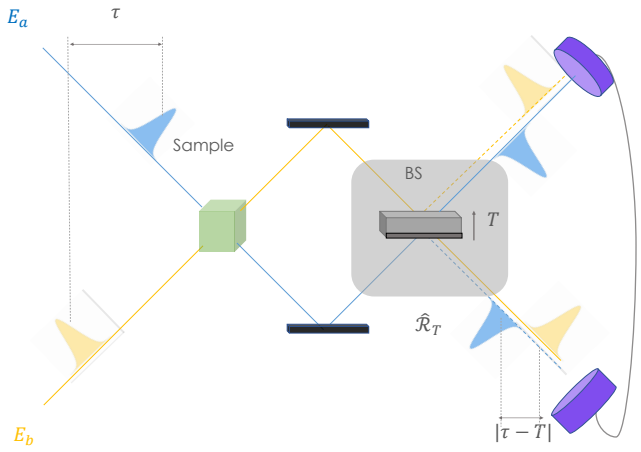

Figure 3. **OTOC detection via a Hong-Ou-Mandel interferometer**. Two quantum probes arranged in space-time wave-packets with relative delay time τ. Then the photons interact with matter (sample), and transformed using BS introducing several possible propagation trajectories of light-matter interaction in a Hong-Ou-Mandel interferometer configuration. The photons are time-resolved and measured in coincidence, forming matter correlation function on a wiggling time contour.

be computed by Eq. 5, by simultaneous annihilation of two photons from both sides of the density operator

$$\mathcal{O}_{t_a,t_b}\left(\boldsymbol{\mathcal{E}},\boldsymbol{\mathcal{E}}^{\dagger}\right)= \quad (6)$$
$$\mathcal{E}^{\dagger}_{R,a}(\boldsymbol{r}_at_a)\,\mathcal{E}^{\dagger}_{R,b}(\boldsymbol{r}_bt_b)\,\mathcal{E}_{L,b}(\boldsymbol{r}_bt_b)\,\mathcal{E}_{L,a}(\boldsymbol{r}_at_a).$$

Eq. 6 projects the two-photon subspace of the density operator as a function of time at two designated detection positions $\{\boldsymbol{r}_a,\boldsymbol{r}_b\}$, annihilating two photons from the left and right. Crucially, both modes (a,b) are measured at the detection plane, and require change of basis with respect to the interaction plane, using the coupling Hamiltonian $\mathcal{H}_{\mu\phi}(t)=\boldsymbol{V}(\boldsymbol{r},t)\cdot\boldsymbol{E}(\boldsymbol{r},t)$ in the interaction-regime basis, and $\boldsymbol{V}=\boldsymbol{\mu}+\boldsymbol{\mu}^{\dagger}$ is the dipole operator (see Sec. S1 and S2 of the SM). A nonvanishing signal is recorded only if two photons are detected. The lowest nonvanishing order contributing to the signal (apart from noninteracting background) includes four events, the two modes are annihilated then created as a result of the interaction with the sample. Multiple processes contribute to the overall signal, however, we are interested to demonstrate a contribution which results in OTOC. Such contributions appear for example by considering the process displayed in Fig. 2a, followed by interferometry from the sample to the detectors which reorders the correlation function as shown in Fig. 2b.

We consider the two-photon initial state of light $|\Psi_0\rangle=\int d\omega_ad\omega_b\Phi(\omega_a,\omega_b)\,a^{\dagger}(\omega_a)\,b^{\dagger}(\omega_b)\,|\text{vac}\rangle$, describing creation of the two modes from the vacuum with amplitude $\Phi(\omega_a,\omega_b)=\phi_a(\omega_a)\,\phi_b(\omega_b)$,and compute the

process amplitude (see Sec. S2 of the SM). When the temporal distribution of the wavepackets ϵ is narrow in comparison to their relative delay τ, and the matter response time, one obtains sufficient temporal resolution to study the OTOC explicitly. We show this by approximating the temporal envelope by delta distributions $\phi_a(t) \to \delta_\epsilon(t-\tau)$, $\phi_b(t) \to \delta_\epsilon(t)$ and obtain

$$\mathcal{C}_{ab}(\tau) \propto \langle V_a(\tau) V_b(0) V_a(\tau) V_b(0) \rangle , \tag{7}$$

for $\tau = 2T$. Eq. 7 clearly reflects the wiggling (forward-backward-forward) time-flow of matter correlation functions carried by an auxiliary probe through an interferometer [64]. We stress that such processes contribute even with no temporal resolution, the delta distributions are invoked purely for illustration purposes. To illustrate this, we have computed the OTOC contribution obtained by applying an entangled pair generated by a spontaneous parametric down-converter pumped using a narrowband beam in Sec. II.B of the SM. Matter information is imprinted in the EM field according to the incidence time. The interaction may occur at various times (which are integrated upon in the interaction picture). The interference of the detected beams depends on equally distributed times dictated by the BS relative displacement, thanks to the linear group velocity of the field. This can be viewed as interfering past and future from the matter point of view (in the absence of losses).

Using this setup, one can measure rates of quantum information scrambling in molecules. Consider for example a two-color measurement whereby two wavepackets, each resonant with different bond (vibrational) or localized electronic state (core electrons) as depicted in Fig. 3. The signal will now carry quantum information regarding "cross talk" of these possibly far-apart channels as well as decoherence processes. Such measurements become particularly interesting for complex bio-molecules, since it can reveal the time and length-scales in which quantum dynamics are important.

The field rotation effect on the time-flow of matter correlation functions, bears a resemblance to the Keldysh rotation. The latter is used to benefit from the linear relations between different kinds of matter Green's functions [65]. Here, the left and right components of the field operators play a role corresponding to forward and backward evolution, by modifying the bra and the ket. Intuitively, the polarization degree of freedom transforms according to Pauli matrices, similar to the augmented Keldysh contour reported in [39]. The correspondence between augmented Keldysh contours and interference of auxiliary fields merits further study in a unified framework.

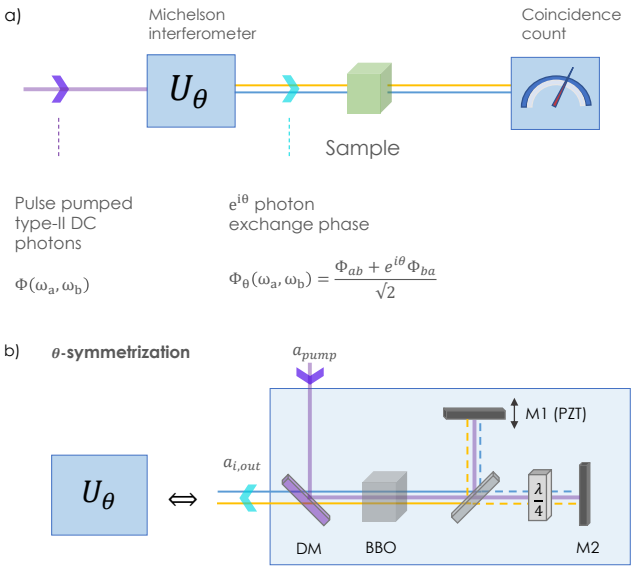

Figure 4. Exchange-phase-cycling scheme. (a) Two-photon exchange phase-cycling setup. The interferometric preparation process attributes θ phase difference with respect to photon exchange, denoted as θ–symmetrization prior to the coupling with the sample. Following the light-matter interaction, the photons are detected in coincidence, scanning the two-photon subspace of the density operator. (b) Implementation of θ-symmetrization via a modified Michelson interferometer (see text).

B. Exchange-phase-cycling protocols; quantum statistics and pathway selectivity

Quantum statistics is known to play a central role in shaping the interference patterns observed in coincidence detection of bosons [66], fermions [67] and fractional charges, e.g., quantum-hall quasiparticles [68]. Indistinguishable photon wavefunctions, such as (ideal) entangled photon pairs, are symmetric with respect to exchange. This is reflected in the generic form of wavefunction using a symmetrized pair amplitude $|\Psi_{\{2\}}\rangle = \frac{1}{\sqrt{2}} \int d\omega_a d\omega_b \left[\Phi(\omega_a, \omega_b) + \Phi(\omega_b, \omega_a)\right] a^\dagger(\omega_a) b^\dagger(\omega_b) |\text{vac}\rangle$, where $a(\omega)$ $\left(a^\dagger(\omega)\right)$ and $b(\omega)$ $\left(b^\dagger(\omega)\right)$ are annihilation (creation) photon operators applied on the vacuum $|\text{vac}\rangle$. In practice, entangled photon pairs are distinguishable owing to variations in the quantum channel responsible for their generation. Orthogonally polarized photon wave packets of entangled pair produced in a type-II parametric down conversion using an ultrashort pump pulse, may be rather distinguishable. Each polarization has a different bandwidth due to the dispersion characteristics of the birefringent crystal [69]. The time-frequency signature invokes some degree of distinguishability resulting in reduced interference contrast due to a nonvanishing exchange phase. Interestingly, the exchange phase of such entangled pair can be set in

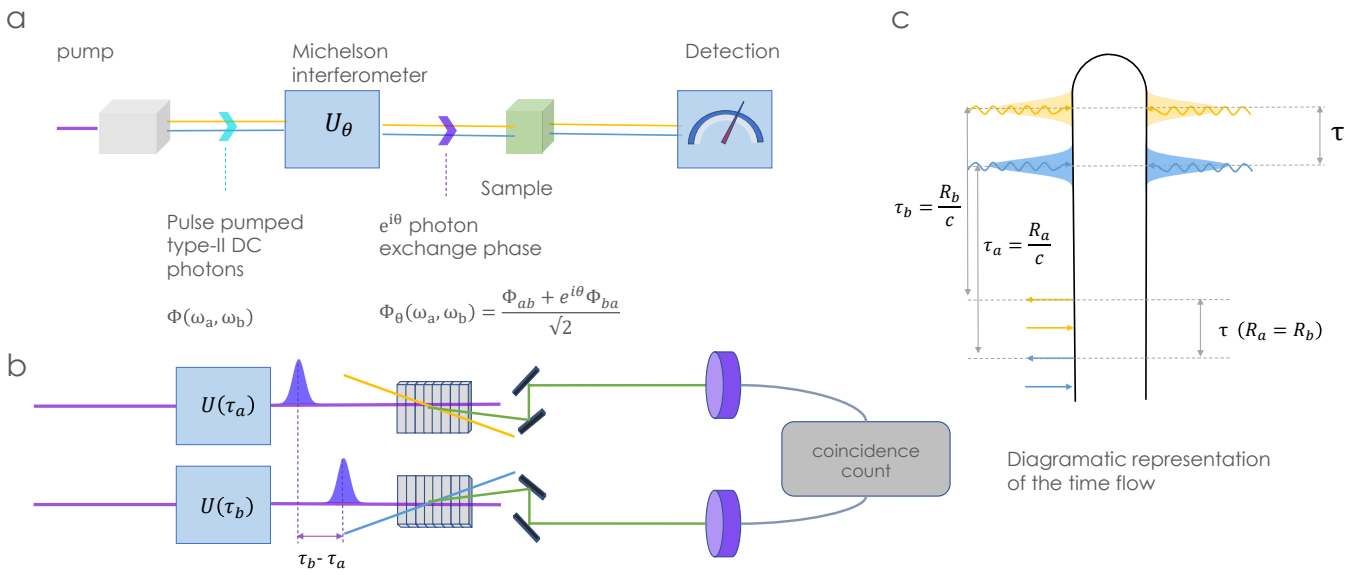

Figure 5. Time-domain switching platform. (a) A θ–symmetrized entangled pair is generated and directed and coupled to a sample. (b) The incident photons (yellow and blue) are separated using a polarization beam splitter (not shown), then scanned in time domain using an up conversion with the same (generating) a delayed pump beam ($U(T_a)$ and $U(T_b)$). The up-converted photons are detected in coincidence. (c) Time-domain diagrammatic description. Emitted light from matter de-excitation undergoes free (retarded) propagation to the detector. Ultrafast time-domain detection scheme with controlled time delay ($\tau = \tau_b - \tau_a$), used as a switch between pathways.

a controlled manner using the Michelson interferometer setup, producing a θ–symmetrized amplitude [69],

$$|\Psi_{\{2\}}\rangle = \int d\omega_a d\omega_b \Phi_\theta(\omega_a, \omega_b)\, a^\dagger(\omega_a)\, b^\dagger(\omega_b)\, |\text{vac}\rangle, \quad (8)$$

where $\Phi_\theta(\omega_a, \omega_b) = \left[\Phi(\omega_a, \omega_b) + e^{i\theta}\Phi(\omega_a, \omega_b)\right]/\sqrt{2}$. The exchange phase can thus be used to manipulate photonic pathways [70]. The pathway in which photon a is coupled to the matter at time t_1 preceding its entangled counterpart $(\omega_a; t_1) \to (\omega_b; t_2)$, and the opposite trajectory $(\omega_b; t_1) \to (\omega_a; t_2)$, carry a valuable phase difference. Repeating the measurement with different values of θ renders a set of signals from which single light-matter interaction pathways can be isolated (pathway selectivity). Generally, preparation interferometric procedures can extend this notion to an N photons amplitudes. N photons exchange phase cycling procedure introduces $\binom{N}{2}$ independent phases using the amplitude

$$\Phi_{\mathbf{\Theta}}(\omega_1, ..., \omega_N) = \mathcal{N}^{-1} \sum_{\{i,j\}} e^{i\theta_{ij}} \hat{\mathcal{P}}_{ij} \Phi(\omega_1, ..., \omega_N), \quad (9)$$

summing over all pair permutations $\{i, j\}$ with the normalization $\mathcal{N} = \sqrt{\binom{N}{2} + 1}$. $\hat{\mathcal{P}}_{ij}$ is the exchange operator between the i and j photons $\hat{\mathcal{P}}_{ij}\Phi_{\mathbf{\Theta}}(\omega_1, ..., \omega_i, ..., \omega_j, ..., \omega_N) = \Phi_{\mathbf{\Theta}}(\omega_1, ..., \omega_j, ..., \omega_i, ..., \omega_N)$. Generating a set of signals with independent exchange phases, one may independently access different pathways.

C. Time-domain QED – ultrafast pathway switching

Remarkable progress in time domain detection techniques, allows the observation of quantum electrodynamic (QED) processes such as electric-field vacuum fluctuations in subcycle scale [71, 72] and bunching at the femtosecond timescale [73]. This offers novel experimental possibilities, such as unraveling light-matter (spontaneous) pathways and sorting between relaxation mechanisms.

A Liouville pathway represents a distinct time ordering of events. Thus, coincidence measurements with a controlled delay, may prove useful for discriminating light-matter absorption-emission sequences. It is possible to recover the temporal profile of each photon of an entangled pair using setups such as the one reported in [74, 75]. Similar to the exchange-phase-cycling protocols, it relies on distinguishability to sort photonic degrees of freedom at the detection process. In . 5 we demonstrate this principle using polarization sorting of unidirectional entangled photon-pair. Controlled distinguishability can be employed by θ–symmetrization, or by applying more sophisticated single photon phase shaping techniques using electrooptic modulation [76].

All possible pathways contribute to the quantum state of the light-matter system. Elimination of multiple pathways is possible by applying a Fock state with fixed number of photons in conjunction with ultrafast time-domain coincidence detection. To demonstrate this, we consider

two photons $N = 2$ as shown in Fig. 5 that undergo a coupling to matter and then detected in coincidence. Time domain scanning technique is employed based on up-conversion process [74, 75]. By fixing the detection time, only events in which both photons arrive simultaneously are counted. We define the temporally gated coincidence count [77]

$$\mathcal{C}\left(\theta,\bar{t}_a,\bar{t}_b\right)=\int dt_a dt_b \mathcal{D}\left(\bar{t}_a,t_a\right)\mathcal{D}\left(\bar{t}_b,t_b\right)W_B^{(2)}\left(t_a,t_b\right), \quad (10a)$$

$$W_B^{(2)}=\left\langle \mathcal{T}\mathcal{E}_{a,R}^{\dagger}\left(t_a\right)\mathcal{E}_{b,R}^{\dagger}\left(t_b\right)\mathcal{E}_{b,L}\left(t_b\right)\mathcal{E}_{a,L}\left(t_a\right) \right. \quad (10b)$$
$$\left. \times \exp\left\{-\frac{i}{\hbar}\int_{-\infty}^{t^*} du\, H_{int,-}\left(u\right)\right\}\right\rangle .$$

Here $\mathcal{E}_R\left(\mathcal{E}_L\right)$ denotes the electromagnetic field superoperator that acts on a Hilbert space operator A from the right (left), $\mathcal{E}_R A\equiv A\mathcal{E}$ $\left(\mathcal{E}_L A\equiv \mathcal{E}A\right)$. Eq. 10a describes the the time-domain gated coincidence, given by integration over the bare signal given in Eq. 10b weighted by the temporal gating functions $\mathcal{D}_i\left(\bar{t}_i,t_i\right)=\left|F_t\left(t_i,\bar{t}_i\right)\right|^2$ which are determined by the pump temporal envelope. Since both photon emission events are spontaneous, no special meaning is attributed to the arrival time of a single photon, the time difference between detection events reveals the time ordering of emission events. This suggests an additional signal, that can be obtained experimentally by scanning and summing all coincidence events in which the relative pump delay $\tau=\tau_b-\tau_a$ is fixed. This corresponds to integration over the last interaction time of a temporally gated coincidence count, defining the signal

$$\mathcal{S}\left(\tau\right)=\int d\bar{t}_a \mathcal{C}\left(\theta,\bar{t}_a,\bar{t}_a+\tau\right). \quad (11)$$

When the pump is shorter than the measured photons wavepackets as depicted in Fig. 5c,each emission event is associated with a single detection, eliminating reversed order processes contributions in the coincidence count. Strikingly, when applied together with the θ – symmetrized amplitude as in Fig. 5b, the signal is sensitive to the exchange in the order of the interactions (exchanging intermediate blue and yellow arrows). Thus, potentially sorting between pathways in addition to reversed emission discrimination.

D. Time-frequency coincidence of entangled photons

Joint properties of systems described by an entangled state are not necessarily constrained by uncertainty restrictions that apply to single systems. By exploiting some distinguishability handles (polarization, color, etc.), it is possible measure simultaneously conjugate properties in an apparent violation of uncertainty relations,

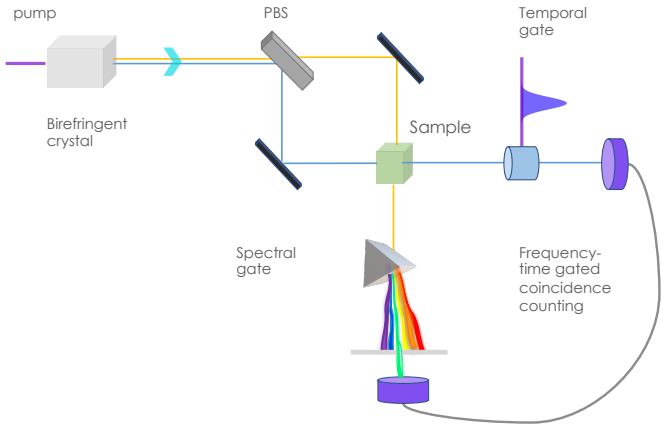

Figure 6. Frequency-time gated coincidence counting setup. Entangled photon pair separated using a polarization beam splitter (PBS). Then coupled to a sample and detected individually. One photon is characterized spectrally while the other in time domain. The photons are ultimately measured in coincidence, producing two dimensional spectra-temporal information with superior joint resolution compared with classical sources.

e.g., joint position-momentum detection of EPR states (See Sec. 4 of the SM). Such phenomenon is easily demystified using the appropriate definitions for conjugate quantities in terms of the many-body wavefunction [78]. These type of nonlocal effects can be further employed to perform quantum microscopy and spectroscopy with unprecedented joint resolutions.

In the setup described in Fig. 6, time-frequency entangled photon pair is coupled to matter. One photon is detected in the time domain using ultrafast up-conversion detection technique, revealing its temporal profile. Its entangled counterpart is spectrally gated, thus recovering its frequency profile. The photons are measured in coincidence,

$$\mathcal{C}\left(\bar{t}_s,\bar{\omega}_i\right)=\left\langle E_{s,R}^{\dagger}\left(\bar{t}_s\right)E_{i,R}^{\dagger}\left(\bar{\omega}_i\right)E_{i,L}\left(\bar{\omega}_i\right)E_{s,L}\left(\bar{t}_s\right) \right. \quad (12)$$
$$\left. \exp\left\{-\frac{i}{\hbar}\int_{-\infty}^{t^*} du H_{\mathrm{int},-}\left(u\right)\right\}\right\rangle .$$

Here $\bar{t}_s$ and $\bar{\omega}_i$ are the scanned time and frequency covered by the respective gates. From the initial frequency correlations of the photons, some knowledge can be obtained regarding the spectral spread of the temporally gated photon, beyond the minimal time-frequency uncertainty. This is possible thanks to the frequency gating of its counterpart, combined with the initial nonlocal correlations. Complementary information is obtained for the frequency gated photon. The two dimensional time-frequency map, potentially exhibits superior joint resolution. The main control parameters are then the gating functions and the initial state of the light (pump bandwidth and crystal length).

IV. SUMMARY

This perspective article surveys several schemes in which interferometry can be combined with quantum states of light in spectroscopy applications. We distinguish between linear and nonlinear interferometric techniques, and describe them using the formalism of linear transformations; relating the input to the output ports. Inclusion of matter degrees of freedom along the electromagnetic flux lines breaks the symmetries of these linear transformation and induces photocurrent that carries matter information. For simplicity, we have considered a colinear propagation direction after the light matter interaction. Phase matching conditions, can generate additional radiation directions induced by nonlinear spontaneous processes, that can be associated with altered transformations. Our algebraic-geometric description of interferometric building blocks, offers a simple explanation for the nonlocal light-matter state after the coupling in terms of vector rotations. These transformations can be employed either before, or after the coupling to matter. These affect the resulting observables, and may give access to different processes as shown above.

Quantum interferometry combined with sequences of light-matter interactions can single out noncausal contributions to nonlinear response functions. Usually such contributions are uniformly summed when classical light probes are involved. Quantum states of light offer sensitivity to the order of events and thus give weights to different pathways. We identify in this case the excess (quantum) information with pathway selectivity. Distinguishability between pathways can be used to separate decay channels in many-body systems, sorting them separately in experiments. OTOC contribute naturally to the interferometric-spectroscopy signals. Distinct OTOC can be extracted in full and measured by ultrafast pulse sequences. Ranging from a single molecule to many-body systems, OTOC tells a story regarding the quantum information scrambling; how a single perturbation that propagates through a quantum system affects different degrees of freedom. Characterizing such behavior becomes increasingly important for materials designed for novel quantum technologies. Also for detecting quantum coherent pathways in systems in which it is not clear whether there are any. From a theoretical point of view, such analysis poses an interesting inference-challenge for few-photon detection of distant atomic processes occurring in curved space-time (which are outside the scope of this perspective).

ACKNOWLEDGMENTS

The support of the National Science Foundation Grant CHE-1953045 is gratefully acknowledged

[1] S. Mukamel, M. Freyberger, W. Schleich, M. Bellini, A. Zavatta, G. Leuchs, C. Silberhorn, R. W. Boyd, L. L. Sánchez-Soto, A. Stefanov, *et al.*, Journal of Physics B: Atomic, Molecular and Optical Physics **53**, 072002 (2020).

[2] K. E. Dorfman, F. Schlawin, and S. Mukamel, The journal of physical chemistry letters **5**, 2843 (2014).

[3] D. A. Kalashnikov, A. V. Paterova, S. P. Kulik, and L. A. Krivitsky, Nature Photonics **10**, 98 (2016).

[4] P. C. Humphreys, M. Barbieri, A. Datta, and I. A. Walmsley, Physical review letters **111**, 070403 (2013).

[5] V. Giovannetti, S. Lloyd, and L. Maccone, Nature photonics **5**, 222 (2011).

[6] F. Herrera, B. Peropadre, L. A. Pachon, S. K. Saikin, and A. Aspuru-Guzik, The journal of physical chemistry letters **5**, 3708 (2014).

[7] C. Silberhorn, P. K. Lam, O. Weiss, F. König, N. Korolkova, and G. Leuchs, Physical Review Letters **86**, 4267 (2001).

[8] O. Varnavski, B. Pinsky, and T. Goodson III, The journal of physical chemistry letters **8**, 388 (2017).

[9] K. E. Dorfman, F. Schlawin, and S. Mukamel, Rev. Mod. Phys. **88**, 045008 (2016).

[10] S. Asban, K. E. Dorfman, and S. Mukamel, Proceedings of the National Academy of Sciences **116**, 11673 (2019).

[11] G. Brida, M. Genovese, and I. R. Berchera, Nature Photonics **4**, 227 (2010).

[12] M. A. Nielsen and I. L. Chuang, *Quantum Computation and Quantum Information: 10th Anniversary Edition* (Cambridge University Press, 2010).

[13] C. W. Helstrom, *Quantum Detection and Estimation Theory*, ISSN (Elsevier Science, 1976).

[14] J. Rarity, P. Tapster, E. Jakeman, T. Larchuk, R. Campos, M. Teich, and B. Saleh, Physical review letters **65**, 1348 (1990).

[15] C.-K. Hong, Z.-Y. Ou, and L. Mandel, Physical review letters **59**, 2044 (1987).

[16] M. Raymer, A. H. Marcus, J. R. Widom, and D. L. Vitullo, The Journal of Physical Chemistry B **117**, 15559 (2013).

[17] A. Kalachev, D. Kalashnikov, A. Kalinkin, T. Mitrofanova, A. Shkalikov, and V. Samartsev, Laser Physics Letters **5**, 600 (2008).

[18] J. Lavoie, T. Landes, A. Tamimi, B. J. Smith, A. H. Marcus, and M. G. Raymer, Advanced Quantum Technologies **3**, 1900114 (2020).

[19] C. M. Caves, Phys. Rev. D **23**, 1693 (1981).

[20] M. Tse, H. Yu, N. Kijbunchoo, A. Fernandez-Galiana, P. Dupej, L. Barsotti, C. D. Blair, D. D. Brown, S. E. Dwyer, A. Effler, M. Evans, P. Fritschel, V. V. Frolov, A. C. Green, G. L. Mansell, F. Matichard, N. Mavalvala, D. E. McClelland, L. McCuller, T. McRae, J. Miller, A. Mullavey, E. Oelker, I. Y. Phinney, D. Sigg, B. J. J. Slagmolen, T. Vo, R. L. Ward, C. Whittle, R. Abbott, C. Adams, R. X. Adhikari, A. Ananyeva, S. Appert, K. Arai, J. S. Areeda, Y. Asali, S. M. Aston, C. Austin, A. M. Baer, M. Ball, S. W. Ballmer, S. Banagiri, D. Barker, J. Bartlett, B. K. Berger, J. Bet-

zwieser, D. Bhattacharjee, G. Billingsley, S. Biscans, R. M. Blair, N. Bode, P. Booker, R. Bork, A. Bramley, A. F. Brooks, A. Buikema, C. Cahillane, K. C. Cannon, X. Chen, A. A. Ciobanu, F. Clara, S. J. Cooper, K. R. Corley, S. T. Countryman, P. B. Covas, D. C. Coyne, L. E. H. Datrier, D. Davis, C. Di Fronzo, J. C. Driggers, T. Etzel, T. M. Evans, J. Feicht, P. Fulda, M. Fyffe, J. A. Giaime, K. D. Giardina, P. Godwin, E. Goetz, S. Gras, C. Gray, R. Gray, A. Gupta, E. K. Gustafson, R. Gustafson, J. Hanks, J. Hanson, T. Hardwick, R. K. Hasskew, M. C. Heintze, A. F. Helmling-Cornell, N. A. Holland, J. D. Jones, S. Kandhasamy, S. Karki, M. Kasprzack, K. Kawabe, P. J. King, J. S. Kissel, R. Kumar, M. Landry, B. B. Lane, B. Lantz, M. Laxen, Y. K. Lecoeuche, J. Leviton, J. Liu, M. Lormand, A. P. Lundgren, R. Macas, M. MacInnis, D. M. Macleod, S. Márka, Z. Márka, D. V. Martynov, K. Mason, T. J. Massinger, R. McCarthy, S. McCormick, J. McIver, G. Mendell, K. Merfeld, E. L. Merilh, F. Meylahn, T. Mistry, R. Mittleman, G. Moreno, C. M. Mow-Lowry, S. Mozzon, T. J. N. Nelson, P. Nguyen, L. K. Nuttall, J. Oberling, R. J. Oram, B. O'Reilly, C. Osthelder, D. J. Ottaway, H. Overmier, J. R. Palamos, W. Parker, E. Payne, A. Pele, C. J. Perez, M. Pirello, H. Radkins, K. E. Ramirez, J. W. Richardson, K. Riles, N. A. Robertson, J. G. Rollins, C. L. Romel, J. H. Romie, M. P. Ross, K. Ryan, T. Sadecki, E. J. Sanchez, L. E. Sanchez, T. R. Saravanan, R. L. Savage, D. Schaetzl, R. Schnabel, R. M. S. Schofield, E. Schwartz, D. Sellers, T. J. Shaffer, J. R. Smith, S. Soni, B. Sorazu, A. P. Spencer, K. A. Strain, L. Sun, M. J. Szczepańczyk, M. Thomas, P. Thomas, K. A. Thorne, K. Toland, C. I. Torrie, G. Traylor, A. L. Urban, G. Vajente, G. Valdes, D. C. Vander-Hyde, P. J. Veitch, K. Venkateswara, G. Venugopalan, A. D. Viets, C. Vorvick, M. Wade, J. Warner, B. Weaver, R. Weiss, B. Willke, C. C. Wipf, L. Xiao, H. Yamamoto, M. J. Yap, H. Yu, L. Zhang, M. E. Zucker, and J. Zweizig, Phys. Rev. Lett. **123**, 231107 (2019).

[21] F. Hudelist, J. Kong, C. Liu, J. Jing, Z. Y. Ou, and W. Zhang, Nature Communications **5**, 3049 (2014).

[22] D. Li, C.-H. Yuan, Z. Y. Ou, and W. Zhang, New Journal of Physics **16**, 073020 (2014).

[23] B. E. Anderson, P. Gupta, B. L. Schmittberger, T. Horrom, C. Hermann-Avigliano, K. M. Jones, and P. D. Lett, Optica **4**, 752 (2017).

[24] M. Manceau, G. Leuchs, F. Khalili, and M. Chekhova, Phys. Rev. Lett. **119**, 223604 (2017).

[25] Y. Shaked, Y. Michael, R. Z. Vered, L. Bello, M. Rosenbluh, and A. Pe'er, Nature Communications **9**, 609 (2018).

[26] G. Frascella, E. E. Mikhailov, N. Takanashi, R. V. Zakharov, O. V. Tikhonova, and M. V. Chekhova, Optica **6**, 1233 (2019).

[27] S. Mukamel, *Principles of Nonlinear Optical Spectroscopy* (Oxford University Press, 1995).

[28] J. Cotler, C.-M. Jian, X.-L. Qi, and F. Wilczek, Journal of High Energy Physics **2018**, 93 (2018).

[29] U. Harbola and S. Mukamel, Physics Reports **465**, 191 (2008).

[30] M. Kryvohuz and S. Mukamel, Phys. Rev. A **86**, 043818 (2012).

[31] M. Kryvohuz and S. Mukamel, The Journal of Chemical Physics **140**, 034111 (2014).

[32] M. O. Scully and K. Drühl, Phys. Rev. A **25**, 2208 (1982).

[33] Y.-H. Kim, R. Yu, S. P. Kulik, Y. Shih, and M. O. Scully, Phys. Rev. Lett. **84**, 1 (2000).

[34] Y. N. O. A.I. Larkin, JEPT **28**, 1200 (1969).

[35] A. Kitaev, in *Proceedings of the Fundamental Physics Prize Symposium* (2014).

[36] S. H. Shenker and D. Stanford, Journal of High Energy Physics **2014**, 67 (2014).

[37] D. A. Roberts, D. Stanford, and L. Susskind, Journal of High Energy Physics **2015**, 51 (2015).

[38] J. Maldacena, S. H. Shenker, and D. Stanford, Journal of High Energy Physics **2016**, 106 (2016).

[39] I. L. Aleiner, L. Faoro, and L. B. Ioffe, Annals of Physics **375**, 378 (2016).

[40] N. Y. Yao, F. Grusdt, B. Swingle, M. D. Lukin, D. M. Stamper-Kurn, J. E. Moore, and E. A. Demler, Interferometric approach to probing fast scrambling (2016), arXiv:1607.01801 [quant-ph].

[41] X. Chen, T. Zhou, D. A. Huse, and E. Fradkin, Annalen der Physik **529**, 1600332 (2016).

[42] B. Yoshida and A. Kitaev, Efficient decoding for the hayden-preskill protocol (2017), arXiv:1710.03363 [hep-th].

[43] I. Kukuljan, S. c. v. Grozdanov, and T. c. v. Prosen, Phys. Rev. B **96**, 060301 (2017).

[44] B. Swingle and D. Chowdhury, Phys. Rev. B **95**, 060201 (2017).

[45] S. Pappalardi, A. Russomanno, B. Žunkovič, F. Iemini, A. Silva, and R. Fazio, Phys. Rev. B **98**, 134303 (2018).

[46] N. Yunger Halpern, A. Bartolotta, and J. Pollack, Communications Physics **2**, 92 (2019).

[47] D. A. Roberts and D. Stanford, Phys. Rev. Lett. **115**, 131603 (2015).

[48] J. R. González Alonso, N. Yunger Halpern, and J. Dressel, Phys. Rev. Lett. **122**, 040404 (2019).

[49] K. A. Landsman, C. Figgatt, T. Schuster, N. M. Linke, B. Yoshida, N. Y. Yao, and C. Monroe, Nature **567**, 61 (2019).

[50] B. Yan, L. Cincio, and W. H. Zurek, Phys. Rev. Lett. **124**, 160603 (2020).

[51] B. Yan and N. A. Sinitsyn, Phys. Rev. Lett. **125**, 040605 (2020).

[52] A. A. Patel and S. Sachdev, Proceedings of the National Academy of Sciences **114**, 1844 (2017).

[53] S. Mukamel, V. Khidekel, and V. Chernyak, Phys. Rev. E **53**, R1 (1996).

[54] Y. Aharonov, S. Popescu, and J. Tollaksen, Physics Today **63**, 27 (2010).

[55] S. Mukamel, Physics Today **64**, 9 (2011).

[56] B. Yurke, S. L. McCall, and J. R. Klauder, Phys. Rev. A **33**, 4033 (1986).

[57] M. D. Reid and D. F. Walls, Phys. Rev. A **31**, 1622 (1985).

[58] W. Du, J. Jia, J. F. Chen, Z. Y. Ou, and W. Zhang, Opt. Lett. **43**, 1051 (2018).

[59] F. R. J. M. Jauch, *The Theory of Photons and Electrons* (Springer, Berlin, Heidelberg, 1976).

[60] R. D. Mota, D. Ojeda-Guillén, M. Salazar-Ramírez, and V. D. Granados, J. Opt. Soc. Am. B **33**, 1696 (2016).

[61] R. D. Mota, M. A. XicotÃ©ncatl, and V. D. Granados, Canadian Journal of Physics **82**, 767 (2004).

[62] C. K. Hong, Z. Y. Ou, and L. Mandel, Phys. Rev. Lett. **59**, 2044 (1987).

[63] R. J. Glauber, Phys. Rev. **130**, 2529 (1963).

[64] S. Asban and S. Mukamel. Out-of-Time-Ordering Matter

Correlators in Quantum Interferometric Spectroscopy, – *to be published* .
[65] A. Kamenev, *Field Theory of Non-Equilibrium Systems* (Cambridge University Press, 2011).
[66] C. K. Hong and L. Mandel, Phys. Rev. A **31**, 2409 (1985).
[67] E. Bocquillon, V. Freulon, J.-M. Berroir, P. Degiovanni, B. Plaçais, A. Cavanna, Y. Jin, and G. Fève, Science **339**, 1054 (2013).
[68] C. de C. Chamon, D. E. Freed, S. A. Kivelson, S. L. Sondhi, and X. G. Wen, Phys. Rev. B **55**, 2331 (1997).
[69] D. Branning, W. P. Grice, R. Erdmann, and I. A. Walmsley, Phys. Rev. Lett. **83**, 955 (1999).
[70] S.Asban and S. Mukamel, Exchange Phase Cycling – pathway selection in Hong-Ou-Mandel Interferometric Spectroscopy. *In preparation*.
[71] C. Riek, D. V. Seletskiy, A. S. Moskalenko, J. F. Schmidt, P. Krauspe, S. Eckart, S. Eggert, G. Burkard, and A. Leitenstorfer, Science **350**, 420 (2015).
[72] C. Riek, P. Sulzer, M. Seeger, A. S. Moskalenko, G. Burkard, D. V. Seletskiy, and A. Leitenstorfer, Nature **541**, 376 (2017).
[73] F. Boitier, A. Godard, E. Rosencher, and C. Fabre, Nature Physics **5**, 267 (2009).
[74] O. Kuzucu, F. N. C. Wong, S. Kurimura, and S. Tovstonog, Phys. Rev. Lett. **101**, 153602 (2008).
[75] J.-P. W. MacLean, J. M. Donohue, and K. J. Resch, Phys. Rev. Lett. **120**, 053601 (2018).
[76] H. P. Specht, J. Bochmann, M. Mücke, B. Weber, E. Figueroa, D. L. Moehring, and G. Rempe, Nature Photonics **3**, 469 (2009).
[77] K. E. Dorfman and S. Mukamel, Phys. Rev. A **86**, 013810 (2012).
[78] J. C. Howell, R. S. Bennink, S. J. Bentley, and R. W. Boyd, Phys. Rev. Lett. **92**, 210403 (2004).
[79] J. D. Cresser, Phys. Rev. A **29**, 1984 (1984).
[80] Detection operators are defined at the detection plane, and thus given in their natural basis.
[81] one can also derive this by first expanding the interaction propagator, then transforming the fields. This will be the formally correct approach. Here we have transformed the field prior to the expansion to express the relative shift between field and matter operators already at the interaction Hamiltonian level in the detection picture. It is confusing to think of the time ordering in terms of the shifted fields and thus here only serves for demonstration purposes.
[82] The fields are described at the same position. The untranslated and dipoles are transforms to the far-field basis, also denoted as detection basis.
[83] S. Mukamel, Phys. Rev. A **77**, 023801 (2008).
[84] K. E. Dorfman, S. Asban, L. Ye, J. R. Rouxel, D. Cho, and S. Mukamel, The Journal of Physical Chemistry Letters **10**, 768 (2019).
[85] D.-I. Lee and T. Goodson, The Journal of Physical Chemistry B **110**, 25582 (2006).
[86] L. Upton, M. Harpham, O. Suzer, M. Richter, S. Mukamel, and T. Goodson, The Journal of Physical Chemistry Letters **4**, 2046 (2013).
[87] O. Varnavski, B. Pinsky, and T. Goodson, The Journal of Physical Chemistry Letters **8**, 388 (2017).
[88] F. Schlawin, K. E. Dorfman, and S. Mukamel, Accounts of Chemical Research **51**, 2207 (2018).
[89] Z. Yang, P. Saurabh, F. Schlawin, S. Mukamel, and K. E. Dorfman, Applied Physics Letters **116**, 244001 (2020).

Interferometric-Spectroscopy With Quantum-Light; Revealing Out-of-Time-Ordering Correlators

— Supplementary Information —

CONTENTS

Appendix S1: Heisenberg picture – field of a dipole

In this section we solve the Heisenberg equation and obtain the displacement operator space-time representation. This provides physical intuition for the seeming irregularity of the in the time ordering of the nonlinear response when quantum interferometers are involved. We begin by closely following the derivation done in [79] for single particle, and then expand it for multiple scatterers. We calculate the displacement operator far from the location of the sample cavity. The sample is composed of multiple scatterers, and is much smaller than the wavelength of the applied field. In this case, the displacement operator coincides with the electric operator within the multipolar expansion. This is a direct result of the localized scatterers model (for more details see Eq. 17 and 18 in [79]).

The field operator far from the sample cavity is given by

$$\boldsymbol{E}\left(\boldsymbol{r},t\right)=\sum_{\boldsymbol{k},s}\sqrt{\frac{2\pi k}{\Omega}}\hat{\epsilon}_{s}\left(\boldsymbol{k}\right)a_{\boldsymbol{k},s}\left(t\right)e^{i\boldsymbol{k}\cdot\boldsymbol{r}}+H.c., \tag{S1}$$

where $\hat{\epsilon}_{s}\left(\boldsymbol{k}\right)$ is the polarization, the speed of light $c=1$, $k=\omega$ and Ω is the quantization volume. We shall solve Heisenberg's equation of motion for the annihilation operator

$$\frac{d}{dt}a_{\boldsymbol{k},s}=i\left[H,a_{\boldsymbol{k},s}\right], \tag{S2}$$

where the coupling is given by $\mathcal{H}_{\mu\phi}=\int d^{3}r\,\boldsymbol{E}\left(\boldsymbol{r},t\right)\cdot\boldsymbol{V}\left(\boldsymbol{r},t\right)$ and the dipole operator is $\boldsymbol{V}\left(\boldsymbol{r}\right)=-e\sum_{\alpha}\left(\boldsymbol{r}_{e,\alpha}-\boldsymbol{r}_{\alpha}\right)\delta\left(\boldsymbol{r}-\boldsymbol{r}_{\alpha}\right)$. $\boldsymbol{r}_{e,\alpha}$ is the position operator of the electron relative to the nucleus positioned in $\boldsymbol{r}_{\alpha}$. This equation admits the formal solution

$$a_{\boldsymbol{k},s}\left(t\right)=a_{\boldsymbol{k},s}e^{-ikt}+\sqrt{\frac{2\pi k}{\Omega}}\int_{0}^{t}d\tau\int_{\mathcal{V}_{\mu}}d^{3}r'\,e^{-i\boldsymbol{k}\cdot\boldsymbol{r}'-ik(t-\tau)}\boldsymbol{V}\left(\boldsymbol{r}',\tau\right)\cdot\hat{\epsilon}_{s}^{*}\left(\boldsymbol{k}\right). \tag{S3}$$

Here $\mathcal{V}_{\mu}$ is the sample cavity volume. Plugging in Eq. S3 into Eq. S1 we obtain two contributions, one from the free evolution and the other due to the dipole acting as a source term,

$$\boldsymbol{E}\left(\boldsymbol{r},t\right)=\boldsymbol{E}_{0}^{(+)}\left(\boldsymbol{r},t\right)+\frac{1}{\left(2\pi\right)^{2}}\sum_{s}\int_{0}^{t}d\tau\int_{\mathcal{V}_{\mu}}d^{3}r'\int_{\mathcal{V}_{k}}d^{3}\boldsymbol{k}k\hat{\epsilon}_{s}\left(\boldsymbol{k}\right)e^{-ik(t-\tau)}\boldsymbol{V}\left(\boldsymbol{r}',\tau\right)\cdot\hat{\epsilon}_{s}^{*}\left(\boldsymbol{k}\right)e^{i\boldsymbol{k}\cdot\left(\boldsymbol{r}-\boldsymbol{r}'\right)}+H.c., \tag{S4}$$

where $\mathcal{V}_{k}$ is the relevant integration domain of the field momentum, and

$$\boldsymbol{E}_{0}\left(\boldsymbol{r},t\right)=\sum_{\boldsymbol{k},s}\sqrt{\frac{2\pi k}{\Omega}}\hat{\epsilon}_{s}\left(\boldsymbol{k}\right)a_{\boldsymbol{k},s}e^{i\boldsymbol{k}\cdot\boldsymbol{r}-ikt}+H.c. \tag{S5}$$

Summing over the polarizations yields

$$\begin{aligned}\Delta E_{i}\left(\boldsymbol{r},t\right)\equiv E_{j}\left(\boldsymbol{r},t\right)-E_{j,0}\left(\boldsymbol{r},t\right)&=\frac{1}{\left(2\pi\right)^{2}}\int_{0}^{t}d\tau\int_{\mathcal{V}_{\mu}}d^{3}r'\int d^{3}\boldsymbol{k}k\left[\sum_{s}\hat{\epsilon}_{s}^{(j)}\left(\boldsymbol{k}\right)\hat{\epsilon}_{s}^{*(i)}\left(\boldsymbol{k}\right)\right]V_{i}\left(\boldsymbol{r}',\tau\right)e^{i\boldsymbol{k}\cdot\left(\boldsymbol{r}-\boldsymbol{r}'\right)-ik(t-\tau)}+H.c.\\&=\frac{1}{\left(2\pi\right)^{2}}\int_{0}^{t}d\tau\int_{\mathcal{V}_{\mu}}d^{3}r'\int d^{3}\boldsymbol{k}k\left[\delta_{ij}-\frac{k_{i}k_{j}}{k^{2}}\right]V_{i}\left(\boldsymbol{r}',\tau\right)e^{i\boldsymbol{k}\cdot\left(\boldsymbol{r}-\boldsymbol{r}'\right)-ik(t-\tau)}+H.c.\end{aligned}$$

The n^{th} order polarization is obtained from the n interactions with the same scatterer, we average over the position of the scatterer (in the cavity volume), and express the n-wave-mixing phase factors explicitly, resulting in the familiar phase-matching factor

$$\Delta E_{i}\left(\boldsymbol{r},t\right)=\frac{1}{\left(2\pi\right)^{2}}\int_{0}^{t}d\tau\int d^{3}\boldsymbol{k}\,k\left[\delta_{ij}-\frac{k_{i}k_{j}}{k^{2}}\right]\int_{\mathcal{V}_{\mu}}d^{3}r'e^{i\left(\boldsymbol{k}\pm\sum_{m}^{n}\boldsymbol{k}_{m}\right)\cdot\boldsymbol{r}'}\left\langle V_{j}\left(\boldsymbol{r}_{\alpha},\tau\right)\right\rangle_{\{n,\boldsymbol{r}_{\alpha}\}}e^{i\boldsymbol{k}\cdot\boldsymbol{r}-ik(t-\tau)}+H.c. \tag{S6}$$

We denote $\Delta\boldsymbol{k} = \boldsymbol{k} \pm \sum_j^n \boldsymbol{k}_j$ and carry the spatial integration – which is possible due to the assumed uniform distribution of scatterers – introducing the phase-matching factor

$$\varphi_V\left(\Delta\boldsymbol{k}\right) \equiv 2^d \int\limits_{\mathcal{V}_\mu} d^3r' e^{i\left(\boldsymbol{k}\pm\sum_j^n \boldsymbol{k}_j\right)\cdot\boldsymbol{r}'}, \tag{S7}$$

where d is the dimension of the cavity (normalization), and obtain

$$\Delta E_i\left(\boldsymbol{r},t\right) = \frac{2^d}{\left(2\pi\right)^2}\int\limits_0^t d\tau \int d^3\boldsymbol{k}\, k \left[\delta_{ij} - \frac{k_i k_j}{k^2}\right] \varphi_V\left(\Delta\boldsymbol{k}\right) \left\langle V_j\left(\boldsymbol{r}_\alpha,\tau\right)\right\rangle_{\{n,\boldsymbol{r}_\alpha\}} e^{i\boldsymbol{k}\cdot\boldsymbol{r}-ik(t-\tau)} + H.c. \tag{S8}$$

Computing the angular integration, using $\int d\Omega \left(\delta_{ij} - \hat{\boldsymbol{k}}_i\hat{\boldsymbol{k}}_j\right) e^{i\boldsymbol{k}\cdot\boldsymbol{r}} = -\left(\partial_{ii}^2 - \partial_i\partial_j\right)\frac{\sin(kr)}{k^3 r}$ then yields

$$\Delta E_i\left(\boldsymbol{r},t\right) = \frac{2^d}{\left(2\pi\right)^2}\int\limits_0^t d\tau \int dk\, k^3 \left[-\left(\partial_{ii}^2 - \partial_i\partial_j\right)\frac{\sin\left(kr\right)}{k^3 r}\right] \varphi_V\left(\Delta\boldsymbol{k}\right) \left\langle V_j\left(\boldsymbol{r}_\alpha,\tau\right)\right\rangle_{\{n,\boldsymbol{r}_\alpha\}} e^{-ik(t-\tau)} + H.c. \tag{S9}$$

Next, we average over the rotations $\left\langle\left(-\partial_{ii}^2 + \partial_i\partial_j\right)\frac{e^{ikr}}{r}\right\rangle_{\text{rotation}} \to \frac{2}{3}k^2\delta_{ij}\frac{e^{ikr}}{r}$ and obtain

$$\Delta E_i\left(\boldsymbol{r},t\right) = \frac{2}{3}\frac{2^d}{\left(2\pi\right)^2}\int\limits_0^t d\tau \int dk \left[k^2\frac{e^{ikr-ik(t-\tau)}}{2ir}\right] \varphi_V\left(\Delta\boldsymbol{k}\right) \left\langle V_i\left(\boldsymbol{r}_\alpha,\tau\right)\right\rangle_{\{n,\boldsymbol{r}_\alpha\}} + H.c. \tag{S10}$$

Here, the backward propagation was eliminated due to causality. We assumed the slowly varying amplitude approximation for the field, extracting the central k_0 from the integration. The phase matching approaches unity for $\Delta\boldsymbol{k} \to 0$. We assume small $\Delta\boldsymbol{k}L$ and carry the integration (considering the phase-matching a multiplicative prefactor)

$$\Delta E_i\left(\boldsymbol{r},t\right) = -\frac{ik_0^2 2^d}{12\pi^2 r}\varphi_V\left(\Delta\boldsymbol{k}\right)\int\limits_0^t d\tau \int dk e^{ikr-ik(t-\tau)} \left\langle V_i\left(\boldsymbol{r}_\alpha,\tau\right)\right\rangle_{\{n,\boldsymbol{r}_\alpha\}} + H.c. \tag{S11}$$

resulting in

$$\Delta E_i\left(\boldsymbol{r},t\right) = -i\frac{2^d\pi}{3\lambda_0^2 r}\left\langle V_i\left(\boldsymbol{r}_\alpha,t-r\right)\right\rangle_{\{n,\boldsymbol{r}_\alpha\}} \varphi_V\left(\Delta\boldsymbol{k}\right)\Theta\left(t-r\right) + H.c. \tag{S12}$$

where we have used the step function $\Theta\left(t\right)$, and defined the central wavelength $\lambda_0 = {}^{2\pi}/_{k_0}$. Equation S12 is constitutes a microscopic derivation for dipole radiation due to nonlinear field interactions – corresponding to Eq. 4.75 in [27]. Averaging over nuclei coordinates gives rise to the structure factor in addition.

Note that the ${}^{\pi}/_2$ factor of the dipole contribution to the radiation is a result of point-like source radiation density of the scatterer while the incoming fields are understood as directional. This phase is closely related to the Gouy phase and require integration of phase-matching condition as well. For a narrow cylinder shaped cavity of length L, the phase matching takes the familiar expression (for which $d = 1$)

$$\varphi_V\left(\Delta\boldsymbol{k}\right) \equiv \varphi_L\left(\Delta\boldsymbol{k}\right) = \frac{L}{2}\text{sinc}\left(\Delta\boldsymbol{k}\frac{L}{2}\right) \tag{S13}$$

resulting in

$$\Delta E_i\left(\boldsymbol{r},t\right) = -\frac{2\pi i}{3\lambda_0^2 r}\left\langle V_i\left(\boldsymbol{r}_\alpha,t-r\right)\right\rangle_{\{n,\boldsymbol{r}_\alpha\}} \left[\frac{L}{2}\text{sinc}\left(\Delta\boldsymbol{k}\frac{L}{2}\right)\right]\Theta\left(t-r\right) + H.c. \tag{S14}$$

Generally, when a single wave is considered, the electric field in the detection plane is given using similar calculation by

$$\boldsymbol{E}\left(\boldsymbol{r},t\right) = \boldsymbol{E}_0\left(\boldsymbol{r},t\right) - i\boldsymbol{V}\left(t-\frac{r}{c}\right)\Theta\left(t-\frac{r}{c}\right), \tag{S15}$$

where we have restored the speed of light to highlight the retardation in the observed time of the dipole oscillation. Here we also assume spatial averaging over scatterer positions, yet express the fact that $\boldsymbol{V}$ maintain operator form. Eq. S15 implies that path transformation of the field is associated with a similar transformation to the respective dipole vector (in the transverse plane). Explicitly, the translation $r \to r + \Delta r$ implies the temporal shift $t \to t - T$ where $T = {}^{\Delta r}/_{c}$. This means that the dipole radiation transforms as a vector as one would naturally expect.

similar results are obtained in nonlinear optics macroscopically by using the Maxwell equations Mukamel [27]. The present derivation is fully microscopic.

Appendix S2: Out-of-Time-Ordering Matter Correlators

1. Definitions

We consider the setup depicted in Fig. S7a, as described in the main text. Two modes $\{E_a, E_b\}$ are prepared in a superposition using BS1, then interact with a sample. Finally the modes are counter rotated by BS2 and measured in coincidence respectively at spacetime coordinates $\{\boldsymbol{r}_a t_a, \boldsymbol{r}_b t_b\}$. The recorded signal is given by simultaneous annihilation of two photons from both sides of the density operator [80]

$$\mathcal{C}_{ab}(T,\tau) = \left\langle \mathcal{T}\mathcal{O}_{t_a,t_b}\left(\boldsymbol{\mathcal{E}},\boldsymbol{\mathcal{E}}^{\dagger}\right)\exp\left\{-\frac{i}{\hbar}\int_{t_0}^{t} du\mathcal{H}_{\mu\phi,-}(u)\right\}\right\rangle \tag{S1}$$
$$\mathcal{O}_{t_a,t_b}\left(\boldsymbol{\mathcal{E}},\boldsymbol{\mathcal{E}}^{\dagger}\right) = \mathcal{E}^{\dagger}_{R,a}(\boldsymbol{r}_a t_a)\,\mathcal{E}^{\dagger}_{R,b}(\boldsymbol{r}_b t_b)\,\mathcal{E}_{L,b}(\boldsymbol{r}_b t_b)\,\mathcal{E}_{L,a}(\boldsymbol{r}_a t_a).$$

Here, the field is broken down into its positive and negative frequency components according to $\boldsymbol{E} = \boldsymbol{\mathcal{E}} + \boldsymbol{\mathcal{E}}^{\dagger}$, and $\mathcal{E}_{L,i}, \mathcal{E}_{R,i}\left(\mathcal{E}^{\dagger}_{L,i}, \mathcal{E}^{\dagger}_{R,i}\right)$ describe electric field annihilation (creation) operators of mode $i \in a, b$, whereby the subscripts (L, R) correspond to left and right operation on the density operator. The signal is obtained by a coincidence measurement of temporally resolved individual photons. We are interested in calculating the contribution due to the diagram given in Fig. S7b, according to the *order of arrival* (detection plane). The field $\boldsymbol{E}(t) = [E_a(t), E_b(t)]^T$ undergoes transformation with respect to the initial state using the rotation matrix (in frequency domain),

$$\hat{\mathcal{R}}_T = \frac{1}{\sqrt{2}}\begin{pmatrix} 1 & ie^{-i\omega T} \\ ie^{i\omega T} & 1 \end{pmatrix}. \tag{S2}$$

Here T is a the relative delay. The initial state of the field is given by, $|0\rangle$

$$|\Psi_0\rangle = \int d\omega_a d\omega_b \Phi(\omega_a,\omega_b)\, a^{\dagger}(\omega_a)\, b^{\dagger}(\omega_b)\,|0\rangle, \tag{S3}$$

the initial state can be represented in the detection basis using the inverse rotation

$$\begin{pmatrix} a(\omega) \\ b(\omega) \end{pmatrix}_{\text{input}} = \frac{1}{\sqrt{2}}\begin{pmatrix} 1 & -ie^{-i\omega T} \\ -ie^{i\omega T} & 1 \end{pmatrix}\begin{pmatrix} a(\omega) \\ b(\omega) \end{pmatrix}_{\text{detection}}.$$

This gives rise to the following transformation

$$a^{\dagger}(\omega_a)\, b^{\dagger}(\omega_b) \to \frac{1}{2}\left[a^{\dagger}(\omega_a)\, b^{\dagger}(\omega_b) - e^{i(\omega_a-\omega_b)T} a^{\dagger}(\omega_b)\, b^{\dagger}(\omega_a) + ie^{-i\omega_b T} a^{\dagger}(\omega_a)\, a^{\dagger}(\omega_b) + ie^{i\omega_a T} b^{\dagger}(\omega_b)\, b^{\dagger}(\omega_a)\right]. \tag{S4}$$

In the derivation below we only keep the terms that contain two modes.

The Interaction Hamiltonian is initially given by $\mathcal{H}_{\mu\phi} = \boldsymbol{E}(t)\cdot\boldsymbol{V}(t)$ is transformed according to $\boldsymbol{E}|_{\text{detected}} = \hat{\mathcal{R}}^{\dagger}\boldsymbol{E}_{\text{interaction}}$, and thus given in the detection basis by [81]. Similarly, the dipole radiation is transformed as a vector

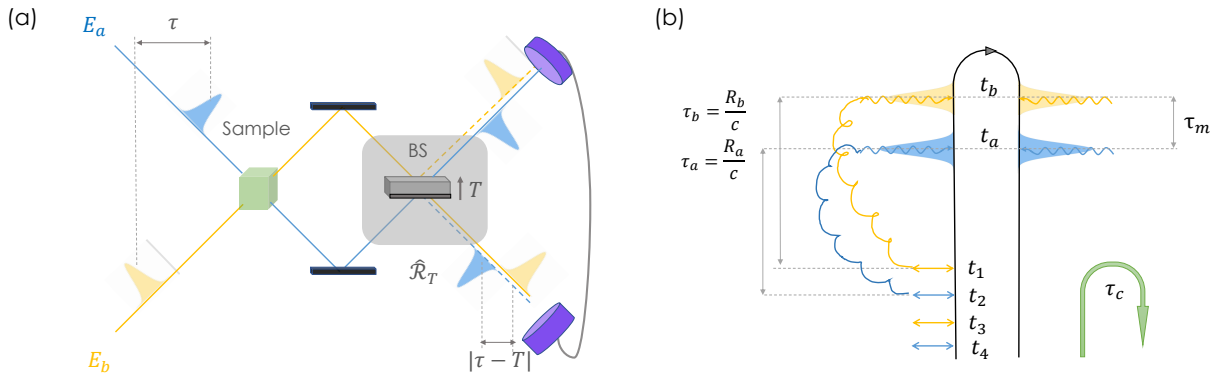

Figure S7. **Demonstration of time-ordering wiggles**. a.) Two photons with τ relative delay time, interact with a sample, then combined a beam-splitter BS. Each photon is scanned in time (t_a, t_b), forming time resolved coincidence detection at two detectors b.) The diagrammatic representation of the considered in the derivation below that contributes to the entire signal, and results in OTOC in some parameter regime.

– see Sec. S1 and the discussion following Eq. S15. Each interaction in the far-field is given by a superposition of terms

$$\begin{aligned}\mathcal{H}_{\mu\phi}(t)|_{\text{detected}} &= \left[\hat{\mathcal{R}}^{\dagger}\boldsymbol{V}(t)\right]\cdot\left[\hat{\mathcal{R}}^{\dagger}\boldsymbol{E}_{\text{detected}}(t)\right] \\ &= \frac{1}{2}\left[\boldsymbol{E}(t)\cdot\boldsymbol{V}(t) - E_a(t+T)\,V_a(t+T) - E_b(t-T)\,V_b(t-T)\right. \quad \text{(S5)} \\ &\quad \left. -iE_b(t+T)\,V_a(t-T) - iE_a(t-T)\,V_b(t+T)\right] \quad \text{(S6)}\end{aligned}$$

where we have omitted the spatial coordinate for brevity, defined $\boldsymbol{E}_{\text{detected}} \equiv \boldsymbol{E}$, and wrote explicitly the polarization operator with respect to its two components $\boldsymbol{V} = (V_a, V_b)^T$. The first two terms constrain the light-matter interaction of individual mode as a single time event. The last two terms account for a mode generated by oscillation of $V_a\,(V_b)$, appearing at the $b\,(a)$ detector – hence the apparent $2T$ relative shift. Having all the ingredients defined, we proceed to the derivation of the contribution of the process in Fig. S7b.

2. Derivation

The coincidence counting of the two fields in the detection picture is given by the time-ordered product (near field),

$$\begin{aligned}\mathcal{C}_{ab}(T) = \mathcal{T}\int_{-\infty}^{t_a} dt_1 \int_{-\infty}^{t_1} dt_2 \int_{-\infty}^{t_2} dt_3 \int_{-\infty}^{t_3} dt_4 \left\langle \mathcal{E}_a^{\dagger}\left(t_a - \frac{R_a}{c}\right)\mathcal{E}_b^{\dagger}\left(t_b - \frac{R_b}{c}\right)\mathcal{E}_b\left(t_b - \frac{R_b}{c}\right)\mathcal{E}_a\left(t_a - \frac{R_a}{c}\right)\right. \\ \left. \times E_b(t_1)\,E_a(t_2)\,E_b(t_3)\,E_a(t_4)\right\rangle \left\langle V_a(t_1)\,V_b(t_2)\,V_a(t_3)\,V_b(t_4)\right\rangle, \quad \text{(S7)}\end{aligned}$$

In the far-field (detection plane), multiple combinations of Eq. S5 contribute [82]. We focus on one contribution

$$\begin{aligned}\mathcal{C}_{ab}^{(I)}(T) = \int_{-\infty}^{t_a} dt_1 \int_{-\infty}^{t_1} dt_2 \int_{-\infty}^{t_2} dt_3 \int_{-\infty}^{t_3} dt_4 \left\langle \mathcal{E}_a^{\dagger}\left(t_a - \frac{R_a}{c}\right)\mathcal{E}_b^{\dagger}\left(t_b - \frac{R_b}{c}\right)\mathcal{E}_b\left(t_b - \frac{R_b}{c}\right)\mathcal{E}_a\left(t_a - \frac{R_a}{c}\right)\right. \\ \left. \times E_a(t_1+T)\,E_b(t_2-T)\,E_a(t_3+T)\,E_b(t_4-T)\right\rangle \left\langle V_a(t_1+T)\,V_b(t_2-T)\,V_a(t_3+T)\,V_b(t_4-T)\right\rangle, \quad \text{(S8)}\end{aligned}$$

Note that time ordering is applied by the integration boundaries. The fields expectation value we are interested in is given by

$$\left\langle \mathbf{1}_{a'},\mathbf{1}_{b'}|\mathcal{E}_a^\dagger\left(t_a-\frac{R_a}{c}\right)\mathcal{E}_b^\dagger\left(t_b-\frac{R_b}{c}\right)\mathcal{E}_b\left(t_b-\frac{R_b}{c}\right)\mathcal{E}_a\left(t_a-\frac{R_a}{c}\right)E_a\left(t_1+T\right)E_b\left(t_2-T\right)E_a\left(t_3+T\right)E_b\left(t_4-T\right)|\mathbf{1}_a,\mathbf{1}_b\right\rangle.$$

We are interested in the following contraction (according diagram in Fig. S7b)

$$\langle \mathbf{1}_{a'},\mathbf{1}_{b'}|\mathcal{E}_a^\dagger\left(t_a-\frac{R_a}{c}\right)\mathcal{E}_b^\dagger\left(t_b-\frac{R_b}{c}\right)\mathcal{E}_b\left(t_b-\frac{R_b}{c}\right)\mathcal{E}_a\left(t_a-\frac{R_a}{c}\right)E_a\left(t_1+T\right)E_b\left(t_2-T\right)E_a\left(t_3+T\right)E_b\left(t_4-T\right)|\mathbf{1}_a,\mathbf{1}_b\rangle$$

resulting in

$$\langle \mathbf{1}_{a'},\mathbf{1}_{b'}|\mathcal{E}_a^\dagger\left(t_a-\frac{R_a}{c}\right)\mathcal{E}_b^\dagger\left(t_b-\frac{R_b}{c}\right)|0\rangle\langle 0|\mathcal{E}_a\left(t_a-\frac{R_a}{c}\right)E_a\left(t_1+T\right)|0\rangle\langle 0|\mathcal{E}_b\left(t_b-\frac{R_b}{c}\right)E_b\left(t_2-T\right)|0\rangle\langle 0|E_a\left(t_3+T\right)E_b\left(t_4-T\right)|\mathbf{1}_a,\mathbf{1}_b\rangle.$$

This process corresponds to two interactions with both photons, resulting in two photon populated state which freely propagates from the sample to the detector. We remember that we focus on a single term to express the OTOC contribution and take the limit of large t_a to obtain

$$\begin{aligned}\mathcal{C}_{ab}^{(I)}\left(T\right)=&\int_{-\infty}^{\infty}dt_1\int_{-\infty}^{t_1}dt_2\int_{-\infty}^{t_2}dt_3\int_{-\infty}^{t_3}dt_4\int d\omega_a^{'}d\omega_b^{'}d\omega_a d\omega_b\Phi^*\left(\omega_a^{'},\omega_b^{'}\right)\Phi\left(\omega_a,\omega_b\right)e^{i\omega_a^{'}\left(t_a-\frac{R_a}{c}\right)}e^{i\omega_b^{'}\left(t_b-\frac{R_b}{c}\right)}e^{-i\omega_a\left(t_3+T\right)}e^{-i\omega_b\left(t_4-T\right)}\\&\times\delta\left(t_a-\frac{R_a}{c}-t_1-T\right)\delta\left(t_b-\frac{R_b}{c}-t_2+T\right)\left\langle V_a\left(t_a-\frac{R_a}{c}\right)V_b\left(t_b-\frac{R_b}{c}\right)V_a\left(t_3+T\right)V_b\left(t_4-T\right)\right\rangle,\end{aligned}\tag{S9}$$

The delta distributions arise due to the curved lines depicted in Fig. S7a. They reflect the free photon propagation from the sample to the detector at the speed of light. Their computation follows similar steps to the ones taken in the derivation of Eq. S15. We assume the detection occurs much later than the interaction process by taking $\left\{t_{a/b},\frac{R_{a/b}}{c}\right\}\to\infty$ such that their difference is finite. Usually we are interested in this point in expressing the signal in frequency domain. Here, we will express the signal in time domain to highlight the time ordering of the correlation function by taking the frequency integrals first,

$$\begin{aligned}\mathcal{C}_{ab}^{(I)}\left(T\right)\propto&\int_{-\infty}^{t_b-\frac{R_b}{c}+T}dt_3\int_{-\infty}^{t_3}dt_4\Phi^*\left(t_a-\frac{R_a}{c},t_b-\frac{R_b}{c}\right)\Phi\left(t_3+T,t_4-T\right)\\&\times\left\langle V_a\left(t_a-\frac{R_a}{c}\right)V_b\left(t_b-\frac{R_b}{c}\right)V_a\left(t_3+T\right)V_b\left(t_4-T\right)\right\rangle.\end{aligned}\tag{S10}$$

Separating the initial state amplitudes reads

$$\begin{aligned}\mathcal{C}_{ab}^{(I)}\left(T\right)\propto&\int_{-\infty}^{t_b-\frac{R_b}{c}+T}dt_3\int_{-\infty}^{t_3}dt_4\phi_a^*\left(t_a-\frac{R_a}{c}\right)\phi_b^*\left(t_b-\frac{R_b}{c}\right)\phi_a\left(t_3+T\right)\phi_b\left(t_4-T\right)\\&\times\left\langle V_a\left(t_a-\frac{R_a}{c}\right)V_b\left(t_b-\frac{R_b}{c}\right)V_a\left(t_3+T\right)V_b\left(t_4-T\right)\right\rangle,\end{aligned}\tag{S11}$$

To get some physical intuition on the measured dynamics, we consider $\phi_a\to\delta_\epsilon\left(t-\tau\right)$ and $\phi_b\to\delta_\epsilon\left(t\right)$. Plugging in the coincidence count we obtain

$$\mathcal{C}_{ab}^{(I)}\left(T,\tau\right)\propto\left\langle V_a\left(\tau\right)V_b\left(0\right)V_a\left(\tau\right)V_b\left(0\right)\right\rangle,\tag{S12}$$

for $\tau = 2T$. Eq. S12 reflects the out-of-time-ordering correlator (OTOC) – reading from right to left – the time evolution is positive then negative, and finally positive again. Such contributions can be calculated according to the time-contour depicted in Fig. S8. Crucially, for wider photon distributions the OTOC contributes in some intervals.

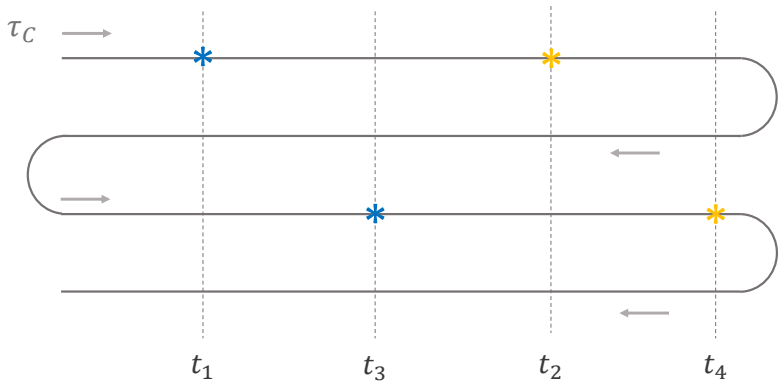

Figure S8. The wiggling-time contour τ_C, along which the matter OTOC demonstrated by Eq. S12 can be computed, as proposed in [39].

The rotating wave approximation

In the above derivation, the field operators took specific form due to the free propagators and inhomogenity (initial photons), while the polarization assumed both components. This means that matter vacuum fluctuations contribute to the over all signal. Now, we invoke the rotating wave approximation in which absorption and emission are associated with decrease and increase of photons respectively. This yields the following modification to the OTOC

$$\mathcal{C}_{ab}^{(I)}(T,\tau) \to \left\langle \mu_a(\tau)\,\mu_b(0)\,\mu_a^\dagger(\tau)\,\mu_b^\dagger(0)\right\rangle. \tag{S13}$$

Implementation using a narrowband entangled photon pair

OTOC contributions appear also when an entangled photon state is considered. We consider a narrowband SPDC entangled photon pair, and compute the coincidence signal. When the entangled pair coherence time T_e is much shorter than the characteristic timescale of the sample (dipole temporal variation), the two photon can be approximated to arrive within a narrow time window [9]

$$\langle 0|E_a(t_1)\,E_b(t_2)\,|\Phi\rangle \propto T_e\delta(t_1-t_2).$$

Plugging this into the coincidence signal, we obtain integrated correlation function that can be divided into OTOC contribution and a time ordered correlator (TOC)

$$\mathcal{C}_{ab}^{(I)}(T,\tau) \propto \Pi\left(\frac{t_a-t_b+2T-\tau}{T_e}\right)\int_0^{2T} dt\,\langle V_a G(\tau)\,V_b G(-t)\,V_a G(\tau)\,V_b\rangle + \text{TOC}. \tag{S14}$$

where we have used the superoperator Green's function $G(t) = \left(-\frac{i}{\hbar}\right)\theta(t)\exp\left(-\frac{i}{\hbar}H_- t\right)$ [83]. Here $\Pi(t) = 1\ \forall t \in (-1/2, 1/2)$ and vanishes out of this interval (approached $\delta(t)$ as $T_e \to 0$) . Clearly the time flow of the first contribution wiggles from positive to negative and back to positive (for $\tau > 0$). The narrow arrival time window eliminates some of the temporal integration. The remaining integration is a result of the spontaneous generation time of the SPDC entangled pair.

Appendix S3: Homodyne vs heterodyne detection

Homodyne detection constitutes a measurement of the signal photons generated from a vacuum (e.g. spontaneous emission). Such signals are relatively weak. The other, heterodyne detection, is based on interference of the weak signal photons with a much stronger local oscillator field. The resulting interferometric pattern has improved signal-to-noise ratio and further provides the phase of the electric field. In classical spectroscopy, i.e. using classical light the signal and local oscillator fields are independently generated and thus, uncorrelated. Combining interferometric tools typically used in quantum optics such as: Mach-Zehnder, Hong-Ou-Mandel and Franson interferometers with quantum light allows to utilize correlations between the signal and local oscillator fields. Rather than measuring a single intensity (photon number $G^{(1)}$), photon statistics measurements (e.g. photon coincidence or intensity variance $G^{(2)}$) can exploit the quantum nature of light. Examples involving two or more intensities include biphoton spectroscopy, ghost imaging, and photon counting spectroscopy all relying on interferometric setups. Photon counting signals may be expressed in terms of multipoint correlation functions of the incoming fields. Spectroscopy is classical if all fields are in a coherent state and the observables are given by normally ordered products of field amplitudes. Field correlation functions may reflect genuine quantum field effects but may also arise from stochastic classical fields. The two should be sorted out. Glauber's celebrated hierarchical correlation formulation of the radiation field aims at field characterization. For spectroscopy applications it must be extended to explicitly include the interaction with matter. Nonlinear optical signals induced by quantized light fields are expressed using *time-ordered* multipoint correlation functions of *superoperators* in the joint field plus matter phase space. These are distinct from Glauber's photon counting formalism which employs *normally ordered* products of *ordinary operators* in the field phase space. Glauber's $G^{(2)}$ function of the incoming light is directly related to its ability to induce correlations in matter. The exploitation of strong correlations with quantum light in nonlinear spectroscopy offers new means for probing complex quantum systems.

Note, that the same interferometer can be used for both homodyne and heterodyne detection of optical signals. For instance, MZ interferometer can detect linear $\chi^{(3)}$ if all field-matter interactions including incoming and detected fields are treated on equal footing. In this case the coincidence signal can be written as a four-point correlation function of the dipole operators. On the other hand, if detected modes are treated separately and traced over the vacuum states, while the incoming modes are traced over the incoming state. In this case the four-point correlation function factorizes into a product of $\chi^{(3)*}\chi^{(3)}$ which yields a homodyne signal.

Appendix S4: Light sources

Quantum light sources are typically classified as such, if they have statistics different from that of a coherent state (e.g., laser). Coherent sources have a Poissonian distribution of photon number. Therefore, the average photon number of a coherent state $|\alpha\rangle$ coincides with its variance $N \equiv \langle N\rangle = \langle \Delta N^2\rangle = |\alpha|^2$. This yields the known average-standard deviation ratio $N/\sqrt{\langle \Delta N^2\rangle} = N^{-1/2}$. The coherent state can be represented as a superposition of Fock states $|n\rangle$. A single photon Fock state is the most basic quantum state which can rely on the benefits of the interferometric setup. Unlike classical states single photon state can interfere with itself giving rise to bunching and antibunching effect, depending on whether interference is constructive or destructive.

Multiphoton Fock states can be generated with a fixed photon number in each spatial mode using the nonlinear interferometric setups discussed above. Such states have very different properties from the single photon Fock state due to their many-body characteristics such as exchange statistics and entanglement. This gives rise to a different spectroscopic signals and yield different phase matching [10, 84].

Entangled states of light are commonly generated via a nonlinear process in which one pump input is converted into two photons, or $\chi^{(2)}$ parametric down conversion (PDC). The most striking properties of entangled light is its vanishing two-photon correlation function $G^{(2)}$ due to strong antibunching, and sub-Poissonian counting statistics. Entangled photons have several important properties stemming from their quantum many-body (more than one) characteristics. While individual photons are constrained to uncertainty relations in the form $\Delta t\Delta\omega \geq 1$ (Fourier uncertainty), the joint probability of the entangled photons is not, e.g. $\Delta(\omega_1+\omega_s)\Delta(t_1-t_2) < 1$. This results in EPR characteristics, which make them perfect candidate for two-photon absorption measurements [85–88]. Second, the parametric process output is sensitive to the pump properties, this yields novel control parameters absent in classical light. For instance, the pump bandwidth σ_p controls the degree of the frequency anti correlations in PDC, and also determines energy conservation. The group velocity in type II PDC of each photon is different, this results in a delay between photon propagating times through the nonlinear crystal and captured by the entanglement time T. EPR correlations are observed when $\sigma_p T < 1$. In two-photon absorption measurements T characterizes an upper bound for the duration in which the system can spend in the intermediate single photon state, before being prompt to double

excited state. Complementarily, σ_p gives spectral bandwidth of the excited two electron/exciton states.

Squeezed light is a multiphoton quantum state composed of photon pairs. Quantum squeezing manifests as a below shot-noise counting error. Such states are typically generated via nonlinear parametric processes such as four-wave mixing. The latter is an interesting scheme, which on its own accord, provides a spectroscopic information about the media where the squeezing is generated via its third order nonlinear response $\chi^{(3)}$. Thus, for the studies of $\chi^{(3)}$ it is not necessary to first generate the squeezed state and then use it to probe the system response, generation itself serves as a spectroscopic probe [89]. The control parameters for the squeezed state include pump and probe phase-matching geometry, intensity of the incoming probe field, four-wave mixing gain and squeezing phase, which is related to the microscopic details of the $\chi^{(3)}$. Cascading interferometric elements allow to improve the degree of squeezing and provides an additional control over the signals.